# Configuring Polarization Singularity Array Composed of C-Point Pairs

Xinglin Wang, Zhiyi Li, Yuan Gao, Zheng Yuan, Wenxiang Yan, Zhi-Cheng Ren, Xi-Lin Wang,
Jianping Ding 🔟, and Hui-Tian Wang

*Abstract*—**The generation and topological configuration of double-layered polarization singularity array (PSA) having paired C-points of opposite topological index through superposing three Laguerre-Gaussian (LG) component beams with orthogonal linear polarization states are demonstrated. The generated PSA beam exhibits diversity in topological geometry and intensity pattern. The topological rule that the zero net topological charge and helicity conservation hold for the entire PSA is also confirmed. Based on our experiment setup consisting of a computer-controlled spatial light modulator (SLM), the PSA morphology can be flexibly customized and dynamically regulated by modulating the parameters of constituent beams. Our scheme provides a convenient device for manipulating polarization singularities and can facilitate the potential applications of singular optics.**

*Index Terms*—**Singular optics, polarization singularity, stokes vortices, orbital angular momentum.**

## I. INTRODUCTION

SINGULAR optics, an important branch of contemporary physical optics, has been widely studied for decades since the wave dislocations was firstly found in 1974 [1]–[5]. Phase singularities in the transverse plane of scalar light beams are usually referred to as optical vortices, where the amplitudes vanish and the phases cannot be defined [1], [6], [7]. In contrast to the scalar light field with uniform polarization, the vector field is characterized by space-variant state of polarization (SOP). In paraxial treatment, the electric field becomes purely transverse and the direction changes in time tracing an ellipse, whose orientation and ellipticity define the local SOP [8]. Polarization singularities are introduced to deal with the singular feature of a polarized field where SOP becomes indeterminate [9]–[12]. Three types of polarization singularities can exist in the transverse electric field, i.e., C-points, points of circular polarization at which the orientation of the polarization ellipse is undefined,

L-lines, lines on which the handedness of the polarization ellipse is undefined, and V-points, points at which the handedness and azimuth are both undefined. In particular, C-points manifest themselves in three kinds of polarization patterns: star, lemon, and monster, all of which can be characterized by the half-integer topological index along a closed loop embracing the singular point.

In recent years, more attention has been paid to polarization singularity arrays (PSAs) due to the increasing interest in their topological morphology and potential applications, and various methods have been carried out to generate such structural beams [13]–[26]. The most common way is to use the interference of three or more non-coplanar plane beams each of which has a predefined SOP, and the interfering waves can be adjusted to realize different PSAs with special topological configurations in their overlapping region [16], [17]. However, such a generation method requires an intricate experimental arrangement that is robust against environmental disturbances. To overcome this issue, dual-phase modulation method has recently been proposed to create regular-shaped (i.e., lattice-like)PSAs [25], in which two phase distributions are encoded into two orthogonal polarization components of the beams, respectively. Another effective method of PSA generation is by means of the superposition of multiple waves carrying orbital angular momentums [14], [24], which has revealed some interesting features of the intensity and polarization distributions, such as the transformation between C-point and V-point during the propagation. Up to now, the PSAs created in this scheme were mainly limited to simple structures, such as single ring-shaped PSA [18]. In this paper, we propose and experientially demonstrate a novel kind of PSA with controllable Stokes vortices by superposing three Laguerre-Gauss (LG) modes; the created PSA is double-layered with particular emphasis on their topological peculiarities. The specialness of our method lies in its flexibility and tunability for regulating PSAs. The PSA morphology can be customized by prescribing appropriate vortex phases and relative amplitude to constituent LG beams and is dynamically regulated by refreshing computer-generated holograms that are encoded on a spatial-light modulator (SLM). In addition, the distribution of polarization singularities can be flexibly regulated by modulating the parameters of constituent beams.

The paper is organized as follows. The theory of PSA formation and its topological analysis are given in Section II. We describe the experimental setup and present the results of PSA generation in Section III. In this section, we demonstrate how to

The authors are with the National Laboratory of Solid State Microstructures and School of Physics, Nanjing University, Nanjing 210093, China (e-mail: wxldreamfly@ahpu.edu.cn; 2226489820@qq.com; 707848936@qq.com; yuanzheng945945@163.com; benson_yan_scut@qq.com; zcren@nju.edu.cn; xilinwang@nju.edu.cn; jpding@nju.edu.cn; htwang@nju.edu.cn).

conveniently configure the PSA by adjusting constituent beams. The concluding remarks of the paper are given in Section IV.

## II. THEORETICAL ANALYSIS AND NUMERICAL SIMULATION

Scalar LG modes are paraxial solutions of the scalar Helmholtz equation in cylindrical coordinate systems [27], and the monochromatic wave function is characterized by the radial index $p$ and azimuthal index $m$ in the form of $E_{p,m}(r, \phi, z) = Y_{p,m}(r, z) \exp(im\phi)$ with

$$Y_{p,m}(r, z) = \sqrt{\frac{2p!}{\pi(p+m)!}} \frac{1}{w(z)} \left[\frac{\sqrt{2}r}{w(z)}\right]^{|m|} L_p^{|m|}$$
$$\times \left[\frac{2r^2}{w^2(z)}\right] \exp\left[\frac{-r^2}{w^2(z)}\right]$$
$$\cdot \exp\left\{-\frac{ikr^2}{2R(z)} - ikz + i(2p + |m| + 1)\psi(z)\right\} \quad (1)$$

where $R(z) = (z^2 + z_R^2)/z$ is the radius of curvature of the wavefront, $w(z) = w_0\sqrt{1 + (z/z_R)^2}$ with $w_0$ being the beam radius at the waist and $z_R = kw_0^2/2$ being the Rayleigh range, $\psi(z) = \tan^{-1}(z/z_R)$, $L_p^{|m|}$ denotes the general Laguerre polynomial, and $k = 2\pi/\lambda$ is the wavevector with $\lambda$ being the wavelength.

In order to generate the composite polarization singularities, we propose to coaxially superposing three LG beams with the same waist parameters. The resultant optical field can be written in the form of Jones vector as

$$\mathbf{E}(r, z, \phi) = \begin{pmatrix} E_x \\ E_y \end{pmatrix}$$
$$= \begin{pmatrix} Y_{p_1,m_1}(r, z)e^{im_1\phi} + Y_{p_2,m_2}(r, z)e^{im_2\phi} \\ A Y_{p_3,m_3}(r, z)e^{im_3\phi}e^{i\delta} \end{pmatrix} \quad (2)$$

where $A$ is a constant to control the relative amplitude of the orthogonal components $E_x$ and $E_y$, and the initial phase difference between them is defined as $\delta$. An effective way to understand the polarization singularities associated with any two-dimensional field is made in terms of normalized Stokes parameters, which are expressed as

$$S_0 = |E_x|^2 + |E_y|^2$$
$$S_1 = S_0^{-1}(|E_x|^2 - |E_y|^2)$$
$$S_2 = S_0^{-1}2\text{Re}(E_x^* E_y)$$
$$S_3 = S_0^{-1}2\text{Im}(E_x^* E_y) \quad (3)$$

where $E_x$ and $E_y$ are the two orthogonal components in the Cartesian coordinate basis. By using the Stokes parameters, one can construct the complex Stokes fields that in particular are useful for analyzing the polarization singular characteristic of light field [10], which are defined as

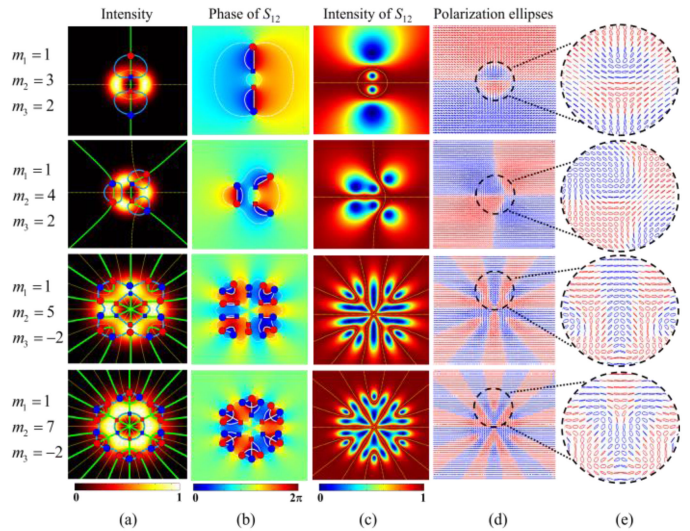$$S_{jk} = S_j + iS_k \quad (j \neq k \in [1, 2, 3]) \quad (4)$$



Fig. 1. Topological configurations of the synthetic field with different component TCs (rows 1–4). First column: Intensity distribution of the synthetic field with embedded C-points; the blue, green and yellow curves represent the contours of $S_1 = 0$, $S_2 = 0$, and $S_3 = 0$, respectively; the red and blue dots marks the RH and LH C-points, respectively. Second column: Stokes phase of the complex field $S_{12}$ showing C-points connected by equal-phase contours. Third column: Intensity pattern of the complex field $S_{12}$ showing L-lines. Fourth column: Polarization ellipses distribution. Fifth column: Magnified version of the circled region in the fourth column.

In these constructed complex Stokes fields a Stokes phase is defined as $\varphi_{jk} = \tan^{-1}(S_k/S_j)$ and establishes a connection between the polarization singularities and the so-called Stokes vortices characterized by the Stokes indices $\sigma_{jk} = (\Delta\varphi_{jk})/2\pi$ with $\Delta\phi_{jk}$ being the accumulated Stokes phases around the singularities. According to the relation between the polarization singularities and the phase vortices in the complex Stokes fields, C-points and V-points appear as the phase vortices in $S_{12}$ Stokes field, where $S_1 = S_2 = 0$ for C-points and $S_1 = S_2 = S_3 = 0$ for V-points, while L-lines occur at the contour of $S_3 = 0$. In what follows, we use the linear polarization basis to theoretically analyze and experimentally perform the generation and topological configurations of the proposed double-layered PSA.

Based on the above theory, we begin with the numerical simulation of the synthesized field expressed by (2) and analyze the polarization singularity in the resultant field. For the comparability between the numerical simulation and experimental demonstration, the waist radii of the three LG constituent beams are chosen to be the same value as $w_0 = 0.6$ mm so that they have same transverse scale and create polarization singularities in desired region of the cross section. Other parameters to be specified in (2) include $A = 1$, $\delta = 0$, and $\lambda = 532$ nm. In addition, we restrict the radial index of three LG modes to be $p = 0$, because it enables a simple but highly adaptable formation of PSA arrays, as will be demonstrated below. Fig. 1 presents the synthesized field from four kinds of combinations of TCs ($m_1$, $m_2$, $m_3$) that are endowed in the three LG constituent beams, showing composite topological configurations of the polarization singularities. To highlight our main results, the case of $m_1 = m_2$,

leading to the only orthogonal superposition of two canonical LG modes, which can be inferred from (2), is not taken into account herein. Columns (a)–(d) display the intensity distribution of the resultant field, the Stokes phase $\varphi_{12}$, the intensity of the complex Stokes field $S_{12}$, and the polarization ellipses, respectively. The C-points and L-lines are embedded in the resultant field and are mapped in the subfigures in column (a); and the C-points locate at the crossings of $S_1 = 0$ (blue solid curves) and $S_2 = 0$ (green solid curves) marked by small circle and square dots, while the L-lines locate at $S_3 = 0$ (yellow dotted curves), separating regions of RH and LH polarization (cf. column (d)). We also use the red and blue color to discriminate between RH C-points ($S_3 = +1$) and LH C-points ($S_3 = -1$), respectively. Column (e) gives the magnified version of local polarization distribution shown in column (d). We can find that the double-layered off-axis PSA are generated as shown in columns (a) and (b) of Fig. 1, where the circle dots mark the location of outer C-points, and the square dots stand for the inner ones accordingly; there exist $|m_3 - m_2|$ pairs of outer C-points and $|m_3 - m_1|$ pairs of inner C-points in the resultant field. As is known, C-points can exist at any intensity of the field, which implies that one cannot determine them by checking the intensity pattern. In contrast, the constructed complex Stokes field $S_{12}$ provides a convenient way to observe C-points by checking the intensity nulls of the complex field, as shown in Fig. 1(c). Moreover, the resultant field exhibits diversity in intensity pattern and topological geometry, differing from those reported in previous works, where the phase singularities or polarization singularities usually distribute along ring trajectories [18], [28]. For example, maps in rows 3 and 4 of Fig. 1 show that the outer C-points of the underlying field locate along quadrilateral-like and hexagon-like trajectories, respectively. Worth emphasizing is that the morphology of polarization singularities is governed by the TCs of constituent beams and thus the positions and number of polarization singularities can be easily tuned by adjusting the parameters of constituent beams.

Next, let us focus on the C-point pair composed of two adjacent outer or inner C-points, which are connected by equal-Stokes-phase contours (three contours at $\varphi_{12} = \pi/3$, $\varphi_{12} = 2\pi/3$, and $\varphi_{12} = 4\pi/3$ as example are shown in column (b) of Fig. 1) and meanwhile separated by L-lines (cf. columns (a) and (c)). Obviously, the sign rule that a constant azimuthal line should pass alternatively through two vortices of TC $+1$ and $-1$ in a Stokes field is satisfied here [29], [30], that is to say, a lemon-type and a star-type C-points form a C-point pair and the star-only or lemon-only fields PSAs cannot solely exist. Furthermore, the handedness of the two paired C-points are always of opposite states, rendering null the TC sum of the entire PSA. It should be mentioned that such an interesting result is also reported in [20], where a lemon-type C-points array and a V-points array interlace with each other and the TC index of the PSA becomes zero. The topological geometry of the resultant field can be clearly seen by further checking polarized ellipses around the respective singularities, as shown in columns (d) and (e) of Fig. 1. The above numerical results lead us to the conclusion that the total TC and handedness are conserved in
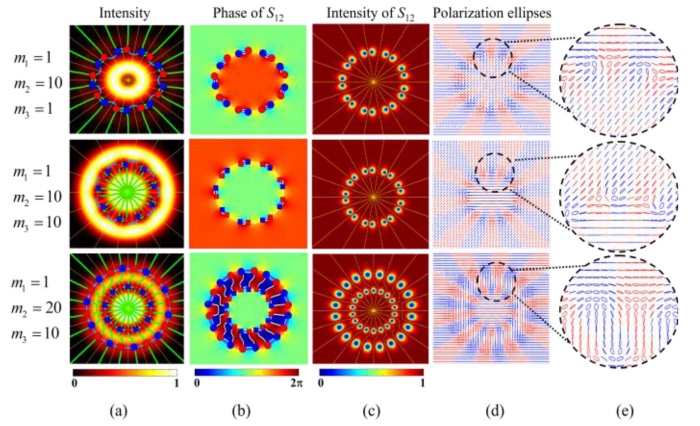


Fig. 2. Simulation of PSAs with different component TCs (rows 1–3). First column: intensity distribution with embedded C-points and L-lines. Second column: Stokes phase of the complex field $S_{12}$ showing C-points connected by equal-phase contours. Third column: Intensity pattern of the complex field $S_{12}$ showing L-lines. Fourth column: Polarization ellipses distribution. Fifth column: Magnified version of the circled region in the fourth column. The red dots, squares, and ellipses denote the right handedness, whereas blue ones correspond to left-handedness.

such a structured synthetic field regardless of the component TCs.

In order to endow the proposed PSAs with more polarization singularities, we choose the component beams having bigger TC difference between them. The corresponding numerical results are presented in Fig. 2. We can observe from the first row that, when $m_1 = m_3$ and $m_2 \neq m_3$, the inner polarization singularities disappear and, therefore, only a outer PSA is created. On the contrary, an inner PSA appears in the case of $m_2 = m_3$ and $m_1 \neq m_3$ shown in the second row. If $m_1 \neq m_3$ and $m_2 \neq m_3$ a double-layered PSA is created as shown in the third row. It is worth noting that the C-points pairs embedded in such a double-layered PSA can be more clearly seen when increasing the corresponding differences in TCs; the corresponding Stokes phase, intensity of the complex field, and elliptical-polarized patterns shown in columns (b)–(e) also reflect this trend.

## III. EXPERIMENTAL RESULTS

To create the proposed PSAs, a vector field generator reported in our previous work [31]–[33] are established, which is a 4-f system composed of two lens L1 and L2 with focal lengths being 400 mm and 300 mm, respectively, as illustrated in Fig. 3. A linear polarized and collimated laser beam with 532nm wavelength illuminates a phase-only spatial light modulator (SLM) (HOLOEYE Leto, 6.4 um pixel pitch, 1920×1080), which loads a computer-generated hologram that encodes the Fourier angular spectrum of the desired PSA field. The two +1st orders (in x- and y-direction) diffraction lights leaving from the SLM are turned into linearly polarized (LP) at 45° with respect to the x-direction by a half wave plate (HWP) and are then converted by an assembled HWP into the x-linearly polarized (XLP) and y-linearly polarized (YLP) components, where the two fast axis directions are set to be 22.5° and 67.5° with respect to the
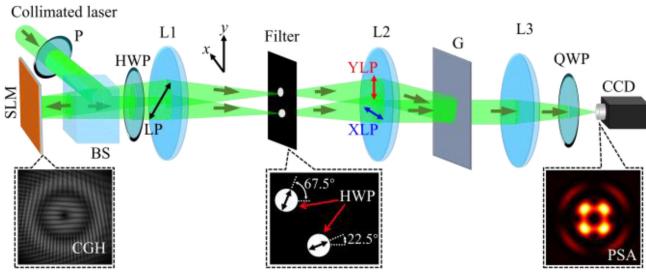
Fig. 3. Schematic of the 4-f optical set-up for creating PSAs. The vector field generator outputs an optical field containing the desired PSA. P: Polarizer; BS: Beam splitter; HWP: Half wave plate; G: Ronchi grating; QWP: Quarter wave plate; CCD: Polarization camera.
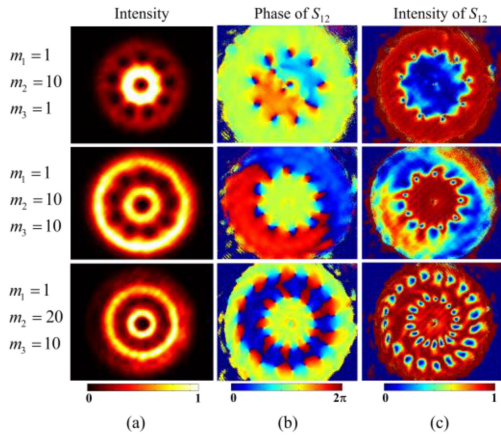


Fig. 4. Experimentally created single- and double-layered PSAs.



Fig. 5. Dependence of double-layered PSA on the relative amplitude factor $A$ of the orthogonal component beams. Rows 1–3 correspond to the cases where the amplitude factor remains constant, while rows 4–6 are responsible for the amplitude factor that varies azimuthally. Other parameters: $m_1 = 1$, $m_2 = 20$, $m_3 = 10$, and $\delta = 0$.

$x$-direction, respectively, thus forming the angular spectra of $E_x$ and $E_y$ expressed in (2). The two component beams are collinearly recombined at the rear focal plane of the second lens L2 by a Ronchi grating, and are finally Fourier transformed into the desired PSA field at the focal plane of a focusing lens L3 with focal length $f = 200$ mm. A polarization camera (4D TECHNOLOGY PolarCam, 3.45 um pixel pitch, 2464 × 2056) – charge coupled device CCD)incorporated with a pixelated linear polarizer array having four discrete polarizations (0°, 45°, 90°, 135°), is used to detect the resultant field and extract the Stokes parameters with the help of a quarter wave plate (QWP) placing in front of the camera.

As a first example of experimental demonstration, we generate the optical field corresponding to the simulated one shown in Fig. 2. The experimental results are shown in Fig. 4, agreeing well with the numerical simulations and thus confirming the realizability of the both single- and double-layered PSAs.

In the second experiment, we focus on how to manoeuvre the double-layered PSA geometry through adjusting the relative amplitude of constituent orthogonal components expressed in (2). The simulation and experimental results are shown in Fig. 5. From the phase and intensity maps of the Stokes field shown in row 1 through row 3, we can clearly see that, with increasing the amplitude, $A$, of the $y$-component beam, the radial spacing between the double-layered PSA gradually increases. Inspired by this effect, we try to construct azimuth-variant double-layered
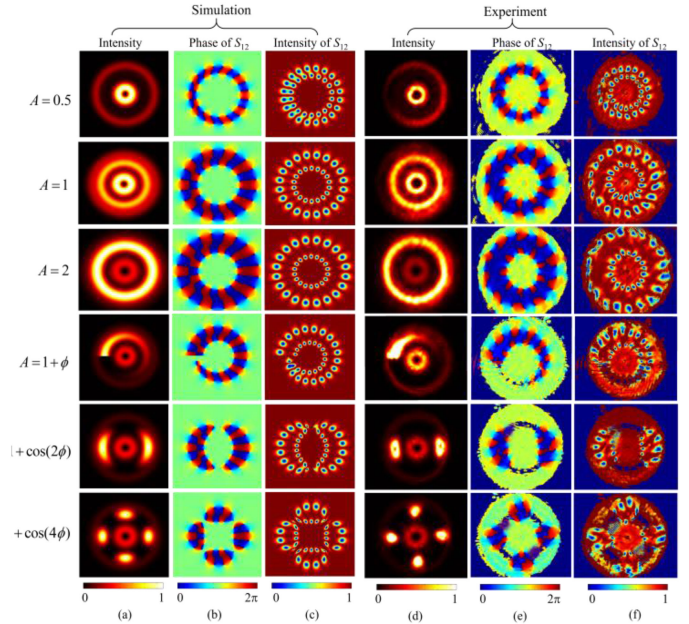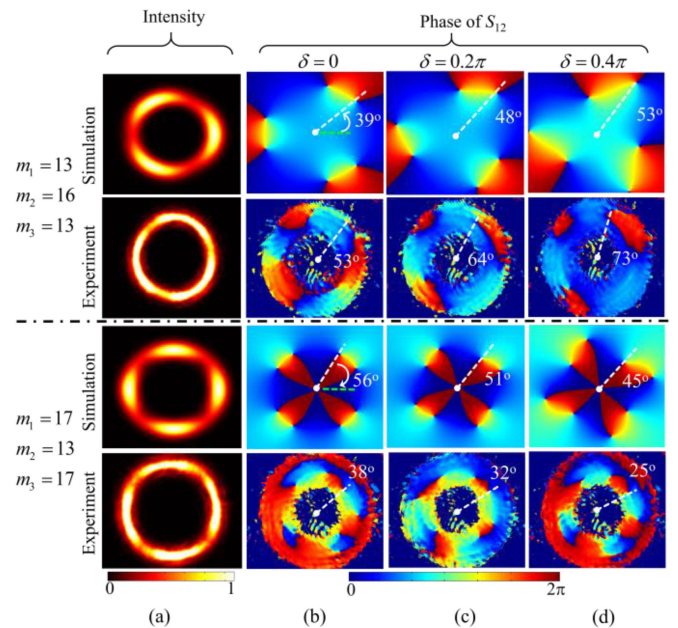


Fig. 6. Numerical results (rows 1 and 3) and corresponding experimental demonstration (rows 2 and 4) of the azimuthal variation of polarization singularities with changing the initial phase difference. Column (a): Intensity distribution at $\delta = 0$. Columns (b)–(d): The corresponding Stokes phase for three initial phase differences of the orthogonal component beams, i.e., $\delta = 0$, $\delta = 0.2\pi$, and $\delta = 0.4\pi$, respectively. The white dashed lines connect a specific singular point and center of the map, rotating along the direction marked by the arc arrow.

PSA patterns by setting a azimuth-dependent amplitude, $A(\phi)$, to the $y$-component beam. Rows 4–6 present the simulation and experimental results for a linear function and two periodic functions with different periods, i.e., $A = 1 + \phi$, $A = 1 + \cos(2\phi)$, and $A = 1 + \cos(4\phi)$, respectively. From row 4 it can be seen that the spacing of the double-layered PSA varies linearly in the azimuthal direction due to the linear relation of $A = 1 + \phi$. Likewise, the periodic variation of $A(\phi)$ in the azimuthal direction drives the PSA pattern to evolve accordingly, displaying a topological configuration with azimuthally periodic geometry as shown in rows 5 and 6. It is also found that the intensity exhibits a similar petal as the topological configuration, which implies that both the topological configuration and the intensity pattern can be flexibly regulated by adjusting the relative amplitude. Worth emphasizing is that our method enables the topological configuration of PSA to be centrosymmetry breaking, which is in stark contrast to commonly ring-shaped PSAs such as that reported in literature [18].

Finally, we study the impact of the initial phase difference in the orthogonal component beams on the topological configuration of PSAs. We change the initial phase difference $\delta$ in an increment of $0.2\pi$ for two sets of TCs, i.e., ($m_1 = 13$, $m_2 = 16$, $m_3 = 13$) and ($m_1 = 17$, $m_2 = 13$, $m_3 = 17$), in which the inner PSA disappears because of $m_1 - m_3 = 0$. The experimental and simulation results are shown in Fig. 6. We can see that the polarization singularities rotate with increasing the initial phase difference, rotating anti-clockwise for $m_2 - m_3 > 0$ and clockwise for $m_2 - m_3 < 0$, respectively. The all results evidently lead us to the conclusion that the proposed double-layered PSA can be generated and flexibly modulated by adjusting the TCs, relative amplitude, and initial phase difference of the component beams.

## IV. CONCLUSION

In summary, we propose a convenient way to generate the double-layered PSA by orthogonally superposing three linearly polarized vortex LG beams, with particular attention on the topological configures of the synthetic field. In terms of complex Stokes field, we firstly theoretically analyze the topological structure of the synthetic field hosting the peculiarity of double-layered C-point pairs. It is found that the numbers of both the outer and inner C-point pairs are dependent on the difference in TCs of the component beams, thus the single- or double-layered PSAs can be generated with adjusting the TCs of the components, which display diversity in intensity and topological geometry. Moreover, the C-point pairs with opposite topological index and handedness confirms the sign rule which requires that the adjacent C-points on a contour of Stokes phase must have opposite topological index, and the helicity conservation. Furthermore, we experimentally generate single- and double-layered PSAs, and demonstrate by simulation and experiment how to regulate the distribution of PSAs through parameters (relative amplitude and phase, TC) of the orthogonal component beams. Our study provides a convenient device for manipulating polarization singularities and can facilitate the potential applications of singular optics.

## REFERENCES

[1] J. F. Nye and M. V. Berry, "Dislocations in wave trains," *Proc. Roy. Soc. London Ser. A-Math. Phys. Eng. Sci.,* vol. 336, no. 1605, pp. 165–190, Jan. 1974.

[2] M. R. Dennis, Y. S. Kivshar, M. S. Soskin, and G. A. Swartzlander, Jr, "Singular optics: More ado about nothing," *J. Opt. A: Pure Appl. Opt.*, vol. 11, no. 9, 2009, Art. no. 090201.

[3] M. Soskin, S. V. Boriskina, Y. Chong, M. R. Dennis, and A. Desyatnikov, "Singular optics and topological photonics," *J. Opt.*, vol. 19, no. 1, Jan. 2017, Art. no. 010401.

[4] Y. Shen *et al.*, "Optical vortices 30 years on: OAM manipulation from topological charge to multiple singularities," *Light Sci. Appl.*, vol. 8, Oct. 2019, Art. no. 90.

[5] Q. Wang, C.-H. Tu, Y.-N. Li, and H.-T. Wang, "Polarization singularities: Progress, fundamental physics, and prospects," *APL Photon.*, vol. 6, no. 4, 2021, Art. no. 040901.

[6] N. Shvartsman and I. Freund, "Wave-field phase singularities: Near-neighbor correlations and anticorrelations," *J. Opt. Soc. Amer. A*, vol. 11, no. 10, pp. 2710–2718, Oct. 1994.

[7] I. V. Basistiy, M. S. Soskin, and M. V. Vasnetsov, "Optical wave-front dislocations and their properties," *Opt. Commun.,* vol. 119, no. 5–6, pp. 604–612, Sep. 1995.

[8] M. Born and E. Wolf, *Principles of Optics, 7th (Expanded) Edition*. Cambridge, U.K.: Press Syndicate Univ. Cambridge, 1999, pp. 401–424.

[9] M. R. Dennis, "Polarization singularities in paraxial vector fields: Morphology and statistics," *Opt. Commun.*, vol. 213, no. 4–6, pp. 201–221, Dec. 2002.

[10] I. Freund, "Polarization singularity indices in Gaussian laser beams," *Opt. Commun.*, vol. 201, no. 4–6, pp. 251–270, Jan. 2002.

[11] M. V. Berry, "The electric and magnetic polarization singularities of paraxial waves," *J. Opt. A: Pure Appl. Opt.*, vol. 6, no. 5, pp. 475–481, Apr. 2004.

[12] F. Flossmann, K. O'Holleran, M. R. Dennis, and M. J. Padgett, "Polarization singularities in 2D and 3D speckle fields," *Phys. Rev. Lett.*, vol. 100, no. 20, May 2008, Art. no. 203902.

[13] I. Freund, "Polarization singularities in optical lattices," *Opt. Lett.,* vol. 29, no. 8, pp. 875–877, Apr. 2004.

[14] T. H. Lu, Y. F. Chen, and K. F. Huang, "Generalized hyperboloid structures of polarization singularities in Laguerre-Gaussian vector fields," *Phys. Rev. A,* vol. 76, no. 6, Dec. 2007, Art. no. 063809.

[15] P. Kurzynowski, W. A. Woźniak, and M. Borwińska, "Regular lattices of polarization singularities: Their generation and properties," *J. Opt.*, vol. 12, no. 3, 2010, Art. no. 035406.

[16] P. Kurzynowski, W. A. Wozniak, M. Zdunek, and M. Borwinska, "Singularities of interference of three waves with different polarization states," *Opt. Exp.,* vol. 20, no. 24, pp. 26755–26765, Nov. 2012.

[17] R. Yu, Y. Xin, Q. Zhao, Y. Chen, and Q. Song, "Array of polarization singularities in interference of three waves," *J. Opt. Soc. Amer. A*, vol. 30, no. 12, pp. 2556–2560, Dec. 2013.

[18] S. Vyas, Y. Kozawa, and S. Sato, "Polarization singularities in superposition of vector beams," *Opt. Exp.,* vol. 21, no. 7, pp. 8972–8986, Apr. 2013.

[19] S. Fu, S. Zhang, T. Wang, and C. Gao, "Rectilinear lattices of polarization vortices with various spatial polarization distributions," *Opt. Exp.,* vol. 24, no. 16, pp. 18486–18491, Aug. 2016.

[20] S. K. Pal and P. Senthilkumaran, "Cultivation of lemon fields," *Opt. Exp.,* vol. 24, no. 24, pp. 28008–28013, Nov. 2016.

[21] E. Otte and C. Denz, "Sculpting complex polarization singularity networks," *Opt. Lett.,* vol. 43, no. 23, pp. 5821–5824, Dec. 2018.

[22] S. K. Pal and P. Senthilkumaran, "Lattice of C points at intensity nulls," *Opt. Lett.,* vol. 43, no. 6, pp. 1259–1262, Mar. 2018.

[23] S. K. P. Ruchi and P. Senthilkumaran, "Basis construction using generic orthogonal C-points," *J. Opt.*, vol. 21, no. 8, Jul. 2019, Art. no. 085603.

[24] C. Chang *et al.*, "Tunable polarization singularity array enabled using superposition of vector curvilinear beams," *Appl. Phys. Lett.,* vol. 114, no. 4, Jan. 2019, Art. no. 041101.

[25] P. Kumar, S. K. Pal, N. K. Nishchal, and P. Senthilkumaran, "Formation of polarization singularity lattice through dual-phase modulation," *J. Opt.*, vol. 22, no. 11, Oct. 2020, Art. no. 115701.

[26] D. Mao *et al.*, "Generation of polarization and phase singular beams in fibers and fiber lasers," *Adv. Photon.,* vol. 3, no. 1, Jan. 2021, Art. no. 014002.

[27] L. Allen, M. W. Beijersbergen, R. J. C. Spreeuw, and J. P. Woerdman, "Orbital angular-momentum of light and the transformation of Laguerre-Gaussian laser modes," *Phys. Rev. A,* vol. 45, no. 11, pp. 8185–8189, Jun. 1992.

[28] S. Baumann, D. Kalb, L. MacMillan, and E. J. O. E. Galvez, "Propagation dynamics of optical vortices due to Gouy phase," *Opt. Exp.,* vol. 17, no. 12, pp. 9818–9827, Jun. 2009.

[29] A. Mokhun, M. Soskin, and I. J. O. l. Freund, "Elliptic critical points: C-points, a-lines, and the sign rule," *Opt. Lett.,* vol. 27, no. 12, pp. 995–997, Jun. 2002.

[30] I. Freund, A. Mokhun, M. Soskin, O. Angelsky, and I. J. O. l. Mokhun, "Stokes singularity relations," *Opt. Lett.,* vol. 27, no. 7, pp. 545–547, Apr. 2002.

[31] X.-L. Wang, J. Ding, W.-J. Ni, C.-S. Guo, and H.-T. Wang, "Generation of arbitrary vector beams with a spatial light modulator and a common path interferometric arrangement," *Opt. Lett.,* vol. 32, no. 24, pp. 3549–3551, Dec. 2007.

[32] C. Chang, Y. Gao, J. Xia, S. Nie, and J. Ding, "Shaping of optical vector beams in three dimensions," *Opt. Lett.,* vol. 42, no. 19, pp. 3884–3887, Oct. 2017.

[33] C. Liang *et al.*, "Radially self-accelerating Stokes vortices in nondiffracting Bessel-Poincare beams," *Appl. Opt.,* vol. 60, no. 28, pp. 8659–8666, Oct. 2021.